Journal of Nuclear Materials 393 (2009) 449–458

Contents lists available at ScienceDirect

Journal of Nuclear Materials

journal homepage: www.elsevier.com/locate/jnucmat

Synthesis and characterization of coffinite

V. Pointeau [a], A.P. Deditius [e], F. Miserque [b], D. Renock [a], U. Becker [a], J. Zhang [a], N. Clavier [c], N. Dacheux [c,*], C. Poinssot [d], R.C. Ewing [a]

[a] Department of Geological Sciences, University of Michigan, Ann Arbor, MI 48109-1005, USA
[b] Laboratoire de Réactivité de Surface et Interface, CEA Saclay DEN/DANS/DPC/SCP, 91191 Gif-sur-Yvette, France
[c] UMR5257 CEA/CNRS/UM2/ENSCM, Centre de Marcoule, Bât. 426, BP 17171, 30207 Bagnols-sur-Cèze, France
[d] Department of Radiochemistry and Processes, CEA Marcoule, DEN/DRCP, 30200 Bagnols-sur-Cèze, France
[e] CSIRO, Exploration and Mining, 26 Dick Perry Avenue, Kensington, WA 6151, Australia

ARTICLE INFO

Article history:
Received 14 April 2009
Accepted 30 June 2009

ABSTRACT

Coffinite, $USiO_4$, has been produced by hydrothermal synthesis. The synthesis products, coffinite nanoparticles (50 nm in size) with UO_2 nanoparticles (a few nanometers), are always associated even if they are not always detected by XRD measurements. The formation of coffinite was shown to be very sensitive to several experimental parameters. The most important of these parameters are the pH, which must be in the range 8–9.5, the pressure, which must be below 50 bars, and the reaction conditions, which must be oxygen-free to maintain uranium in its tetravalent oxidation state. XRD and TEM reveal that tetragonal coffinite accounts for more than 90% of the final products while the by-products UO_2 and a Si-rich amorphous phase are also present. The structural formula of the obtained coffinite is close to $USiO_4$ as determined from EMPA ($U_{0.99\pm0.06}Si_{0.97\pm0.07}O_4$). XPS measurements show a peak chemical shift of the U-4*f* core levels by 1 eV toward higher binding energies in coffinite compared with stoichiometric UO_2. The U-$4f_{7/2}$ and U-$4f_{5/2}$ positions in coffinite are found to be near 380.8 ± 0.3 eV and 391.7 ± 0.3 eV, respectively.

1. Introduction

Renewing interest in nuclear energy requires bringing reliable and scientifically sound solutions to manage high level nuclear waste in the back-end of the fuel cycle. Although it is not the legal option in France, direct disposal of spent nuclear fuel (SNF) is considered in other countries like the USA, and must in any case be investigated as a precaution. In a direct disposal repository, most of the radionuclides will be released by UO_2 matrix alteration [1] in a strongly reducing environment (Eh < −180 mV), the main exception being Yucca Mountain. Under these conditions, SNF alteration may proceed after some tens of thousands of years (after the initial stage governed by radiolytic dissolution [2–4]) by corrosion (release of U^{VI}) or, at lower Eh, by chemical dissolution (release of U^{IV}) [5,6]. Dissolved uranium will thereafter reprecipitate as U(IV) secondary phases which could increase the SNF alteration rate and act as a radionuclide sink [7,8]. In many potential host rocks considered for a repository, silica concentrations are high enough to allow silicate precipitation (for instance, Si ~ 10^{-4} mol L^{-1} in the French candidate site – Meuse/Haute–Marne – for a future repository). Coffinite $USiO_4$ is therefore expected to be one of the potential alteration phases precipitating from SNF alteration under reducing Si-rich conditions [10–15]. Indeed, this mineral is widely observed in uranium ore deposits as an alteration phase of uraninite (natural analog of SNF [16]), particularly at Oklo (Gabon) [13,17–19] and Cigar Lake (Canada) [20–23]. Coffinite is also observed as primary uranium mineral in roll-front deposits where uranium precipitates in tight redox fronts as in Kazakhstan [24].

The existence of a compound with the chemical formula $USiO_4$ was first postulated by Goldschmidt [25], by the substitution of U^{4+} for Th^{4+} in thorite $ThSiO_4$. Coffinite was first observed in the La Sal mine, Colorado Plateau [26], and was named after R.C. Coffin (American geologist, pioneer in the study of the uranium deposits in the Colorado Plateau). Coffinite is an orthosilicate, isostructural with zircon ($ZrSiO_4$), thorite ($ThSiO_4$) [27–29], and other actinide silicates at the tetravalent state like Np, Pu, and Am [30]. Coffinite has a tetragonal unit cell with space group symmetry $I4_1/amd$ and $Z = 4$ [31]. In this structure, each U atom is surrounded by 8 O atoms, 4 at a distance of 0.238 nm and 4 at a distance of 0.236 nm. These distances are comparable with those measured in UO_2 (0.236 nm) [32]. The UO_8 polyhedron shares its edges with the SiO_4 tetrahedra along the *c*-axis (Fig. 1).

The chemical formula of coffinite is still controversial with respect to the existence of water molecules or hydroxyl groups. Based on infrared measurements, the first formula shows hydroxyl groups substituting for Si in tetrahedra, i.e. $U(SiO_4)_{1-x}(OH)_{4x}$ [27]. Conversely, more recent studies did not confirm the presence of

* Corresponding author. Tel.: +33 4 66 33 92 05; fax: +33 4 66 79 76 11.
E-mail address: nicolas.dacheux@univ-montp2.fr (N. Dacheux).

0022-3115/$ - see front matter © 2009 Elsevier B.V. All rights reserved.
doi:10.1016/j.jnucmat.2009.06.030

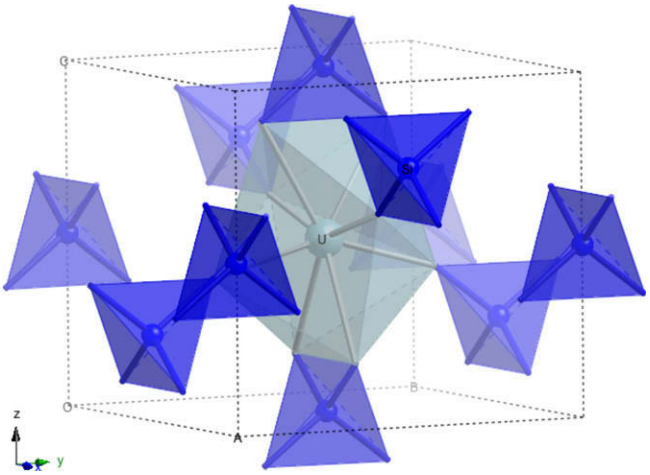

Fig. 1. The structure of coffinite: the UO_8 polygon (grey) shares four oxygen atoms with two tetrahedral SiO_4 (blue) along the *z* axis). (For interpretation of the references to colour in this figure legend, the reader is referred to the web version of this article.)

hydroxyl groups in the coffinite structure; instead an absorption band at 1600 cm^{-1} suggests the presence of molecular water [33–35]. For instance, Zimmer [36] mentioned a significant amount (10–15%) of water in the structure of several natural coffinite samples, while Janeczek and Ewing [12] proposed the formula $USiO_4{\cdot}n$-H_2O, with $n \approx 2$.

There are no experimentally determined thermodynamic properties of coffinite, although some values were selected and validated by Guillaumont et al. in the Thermodynamic DataBase project [9]. All the available thermodynamic data for coffinite have been derived by molecular calculations and/or by analogy with other orthosilicates [37–39]. The Gibbs free energy for the formation of $USiO_4$(cr) is estimated to be -1884 ± 4 kJ mol^{-1} at 298.15 K. However, this value is based on Langmuir's hypothesis which assumed that uraninite and coffinite are in thermodynamic equilibrium and control the silica concentration in the Grant Mineral Belt for an arbitrary silica concentration of 10^{-3} mol L^{-1} [40]. Robit-Pointeau et al. [41] and Grambow and Giffaut [42] suggested that the Grant Mineral Belt equilibrium hypothesis may be erroneous because the silica concentration H_4SiO_4(aq) in the groundwater is more likely controlled by Al-silicates and quartz or chalcedony.

One of the major problems in obtaining accurate thermodynamic data for coffinite lies in the difficulty of synthesizing pure coffinite. Most of the natural samples also contain uraninite, and synthesizing pure coffinite samples without any by-products such as uraninite is challenging. Coffinite was assumed to have been synthesized through hydrothermal techniques by Fuchs and Hoekstra [33], Keller [43] and Mulak [44]. Conversely, Mumpton and Roy [45] did not synthesize coffinite but uraninite and quartz and suggested coffinite may be metastable. Robit-Pointeau [41,46] suggested that (i) either the domain of thermodynamic stability of coffinite occurs in a narrow Eh/pH range, which would be different from the one predicted by the selected thermodynamic data [9], (ii) and/or coffinite precipitation is a kinetically controlled process and requires an unidentified precursor that could involve organic matter as reported from the uranium deposit [10,47,48]. Other coffinite synthesis protocols based on hydrothermal [49,50,7] or dry methods [51,52] are mentioned in the literature. However, only Pishva [49] published XRD results for the final product, which is most likely a mixture of UO_2, U_3O_8, $UO_3{\cdot}2H_2O$ (schoepite) and $Na_2(UO_2)_2(Si_2O_5)_3(H_2O)_4$ (Na-weeksite) based on the published XRD pattern. Most other studies [50,52] identify coffinite only on the basis of the U/Si molar ratio ~1 measured by EDS. Due to the small size of crystals and the likely presence of uraninite and SiO_2 as by-products, this ratio cannot unambiguously attest the presence of coffinite.

The purpose of this study was to develop a reproducible synthesis technique for coffinite that would produce enough material for detailed characterization.

2. Experimental

2.1. Chemicals and apparatus

All reagents were Alfa Aesar analytical-grade products, except the uranium tetrachloride solution, which was obtained from the dissolution of uranium metal chips in hydrochloric acid. First, 2 M hydrochloric acid was used to eliminate the oxides present at the surface of the chips. Then the chips were washed by water then ethanol and finally dissolved in 4 M hydrochloric acid [53]. The acid concentration was adjusted to 6 M to stabilize uranium in its tetravalent oxidation state for a long time. The uranium concentration was estimated to be 0.92 ± 0.02 M using the titration method developed by Dacheux et al. [54,55]. Syntheses were performed under hydrothermal conditions in Parr Instrument autoclaves lined by polytetrafluoroethylene (PTFE) containers (maximum volume of 23 mL). Samples were heated to 250 °C for 24 to 84 h.

Table 1
Effect of different parameters on coffinite precipitation.

Sample label	pH before heating	pH after heating	*T* (°C)	Heating duration (h)	Pressure condition (bar)	Compounds detected by XRD
S1	12	12	250	24	40	UO_3, NaCl, Na_2SiO_3
S2	9	10	250	24	40	Coffinite, uraninite[a]
S3	9.5	10	250	84	40	Coffinite, uraninite[a]
S4	9	n.m.	250	36	40	Coffinite, uraninite[a]
S5	8	n.m.	250	24*	50	Uraninite
S6	8.5	9.5	250	24	40	Coffinite
S7	8.5	n.m.	250	24	40	Coffinite, uraninite[a]
S8	9	9.5	250	36	40	Coffinite, uraninite[a]
S9	8.5	9	250	36	40	Coffinite, uraninite[a]
S10	9	9	250	36	40	Coffinite, uraninite[a]
S11	9	9	250	36	40	Coffinite, uraninite[a]
S12	9	9	250	36	40	Coffinite, uraninite[a]
S13	9	10	250	36	40	Coffinite, uraninite[a]

n.m.: not measured.
* Heating by stage: step for increasing temperature from 25 to 250 °C: 60°/h, 250 °C for 24 h, step for decreasing temperature from 250 to 23 °C: 60°/h, agitation during all the heating process.
[a] Uraninite is detected as a minor phase (between 5 and 10 wt.%).

2.2. Synthesis procedure

Coffinite $USiO_4$ was prepared using a method adapted from the protocol by Fuchs and Hoekstra [33] in an inert glove box under reducing conditions containing N_2(95%)/H_2(5%), to prevent any oxidation of U(IV) to U(VI). Synthesis was performed with excess aqueous silica to favor the complexation of aqueous U(IV) with silica at the expense of hydroxylation, as hydroxylation leads to the precipitation of UO_2. One mmol of UCl_4(aq) dissolved in 5 mL of degassed water was added dropwise to the solution of slightly substoichiometric Na_2SiO_3 dissolved in 5 mL of degassed water. A 2 M NaOH solution was added dropwise to adjust the pH to about 8. The resulting solution was then buffered close to pH = 9 by adding $NaHCO_3$ to obtain a final concentration of 0.5 M carbonate ions. These conditions are summarized in Table 1. The initially formed green gel was poured into two kinds of autoclave and heated for 24–84 h: (i) standard acid digestion bomb or (ii) autoclave equipped with a temperature controller and agitation device. Unlike Fuchs and Hoekstra's protocol [33], the preliminary gel phase was directly used for the precipitation step whereas those authors first eliminated it and only used the supernatant after centrifugation.

2.3. Characterization techniques

XRD powder diffraction analyses were performed using a Scintag diffractometer (Scintag X1, Cupertino, CA) with a Cu Kα (λ = 1.54060 Å) radiation source. An accelerating voltage of 45 kV and a current of 40 mA were used. The XRD data were collected over a 2θ range of 5–90° in 0.02° increments.

Electron microprobe analyses (EMPA) were carried out using a Cameca-SX-100 apparatus with an acceleration voltage of 20 kV and a current intensity of 40 nA for the detection of uranium and silicon and of 20 nA for sodium and chlorine. The following standards were utilized: UO_2 (Mβ ray of uranium), $NaAlSi_3O_8$ (Kα ray of silicon), $NaNbO_3$ (Kα ray of sodium), $BaCl_2$ (Kα ray of chlorine). The counting time was from 10 to 30 s and the beam spot diameter was ~1 μm.

High-resolution transmission electron microscopy (HRTEM) and analytical electron microscopy (AEM) were conducted using JEOL JEM2010F and Philips CM12 electron microscopes. The point to point spatial resolution was 0.14 nm for the JEOL JEM2010F and 0.34 nm for the Philips CM12. The high-resolution (HR) mode revealed the texture and organization of the atomic planes of the final product to be determined at nanometric scale. The Selected area diffraction (SAED) pattern helps to identify the structure of individual grains.

X-ray photoelectron spectroscopy (XPS) analyses were carried out using a VG ESCALAB 220i XL. The X-ray source of the VG ESCALAB 220i XL uses monochromatic Al-Kα radiation with an incident energy of 1486.6 eV. The analyzed surface area was 6 × 7 mm^2. The C 1s peak (adventitious carbon) was as an internal standard and its position was defined to be 285 eV.

3. Results

3.1. XRD characterization

In order to evaluate the influence of several parameters on the formation of coffinite, 13 syntheses (designated S1–S13) were performed with various initial conditions (listed in Table 1). The final products were systematically characterized using XRD. The set of XRD diffractograms is shown in Fig. 2.

The XRD diagrams depict the specific XRD lines of coffinite for all the samples prepared under the initial conditions at pH values between 8 and 9.5 (syntheses S2–S4 and S6–S13). Among these, synthesis S6 shows pure coffinite and does not reveal any impurities with respect to the detection limit of the method, which is 5 vol.%. Conversely, the XRD patterns of samples S2–S4 and S7–S13 reveal additional peaks characteristic of UO_2. Furthermore, a slight continuous background, which is characteristic of amorphous phases, is observed in most of the samples. Rietveld refinements were performed on XRD diagrams of samples S3 and S4 to estimate the ratio between coffinite and UO_2 in the samples. Semi-quantitatively, S3 and S4 were found to contain about 10 wt.% UO_2. On the basis of the full width at half maximum (FWHM) of XRD lines, the grain size of the UO_2 crystals was determined to be about 4 nm.

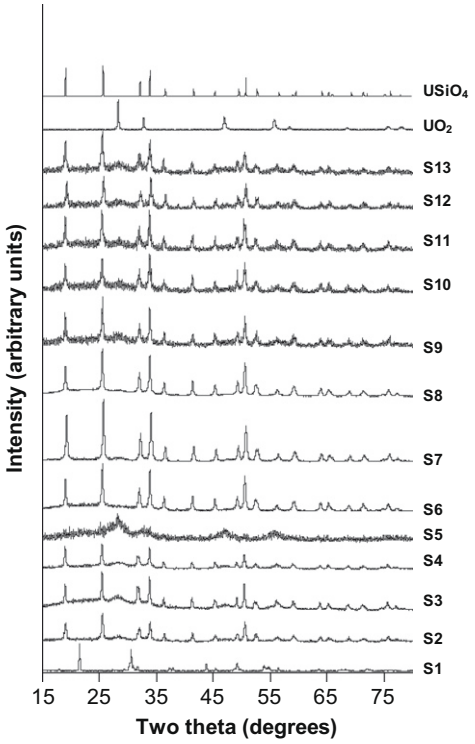

Fig. 2. XRD diagrams of 13 synthesized products compared with coffinite ($USiO_4$) and uraninite (UO_2).

Table 2
Crystallographic data of synthetic coffinite compared to that reported in literature for coffinite, zircon and thorite.

Parameter (Å)	Coffinite $USiO_4$		Zircon	Thorite
	This study	Fuchs and Gebert	$ZrSiO_4$	$ThSiO_4$
$a = b$	7.0135 ± 0.0004	6.981 ± 0.004	6.60	7.13
c	6.2669 ± 0.0006	6.250 ± 0.005	5.98	6.32

The unit cell parameters of coffinite were refined using unit cell refinement software (Table 2), based on the methods described by Holland and Redfern [56]. The unit cell parameters derived for synthetic coffinite ($a = b$ = 7.0135(4) Å and c = 6.2669(6) Å) are within <1% of the values reported by Fuchs and Gebert ($a = b$ = 6.981(4) Å and c = 6.250(5) Å) [28]. These unit cells parameters are also intermediate between the structural parameters of zircon and thorite (Table 2), which is consistent with the relative orders between ionic radii of Zr^{4+} (0.84 Å), U^{4+} (1.00 Å), and Th^{4+} (1.05 Å) in the eightfold coordination.

Increasing the N_2/H_2(5%) pressure to 50 bars during the synthesis of sample S5 caused precipitation of UO_2, an amorphous Si-phase, and only small amounts of coffinite (Fig. 2). Moreover, increasing the pH to 12 during synthesis S1 led to the formation of UO_3 and Na_2SiO_3. Importantly, all attempts of synthesis failed when the reactants were added in the reverse order, i.e. a silica solution was added to uranium solution [46], and only UO_2 was detected.

3.2. EMPA characterization

The three samples of synthetic coffinite, S3, S4, and S6, were selected for detailed characterization to investigate the relation between synthetic coffinite and uraninite (S3 and S4) and reveal the features of pure coffinite (S6) documented by means of XRD.

The back-scattered electron (BSE) images of sample S6 show that the final product consists of patchy, polycrystalline aggregates with heterogeneous BSE Z-contrast (Figs. 3 and 4). Selected representative EMPA data (Table 3) evidence the polyphase feature of the sample since at least three distinct zones could be differentiated on the basis of the analyses. They reveal that the weight percentages of U and Si vary over wide ranges from 64.6 to 71.6 wt.% and from 19.8 to 28.9 wt.%, respectively. The product also contains from 0.2 to 0.7 wt.% Na, with less than 0.1 wt.% Cl. The overall U/Si ratio is low, 0.63 ± 0.07, compared with the expected U/Si ratio of coffinite (i.e. 1.00). This low U/Si ratio clearly indicates excess silicon, which is most probably due to the presence of the Si-rich phase. The line scan along the coffinite aggregate shows an abrupt increase in uranium and decrease in silicon concentrations close to the border of the analyzed aggregate (Fig. 3a and b). Elemental mapping reveals that the darker zones in BSE (aggregates ~10 μm thick) are depleted in U and enriched with Na and Si, thus, a Na–Si-rich phase. In contrast, the second examined aggregate shows larger chemical variations than the first one (Fig. 4a, profile 2) with "darker" areas enriched in Na and depleted in U and Si comparing to the "brighter" areas (Fig. 4d and e).

Sample S3 also consists of polycrystalline aggregates forming grains of about 1–3 mm in size (Fig. 5a). Some of them appear heterogeneous in SEM (Fig. 5b). The EMPA analyses collected from the homogeneous areas, with respect to BSE contrast, reveal that the amounts of U and Si vary from 74.0 to 81.0 wt.% and from 12.6 to 20.9 wt.%, respectively. The sodium and chlorine originating from the synthesis were evaluated to be as high as 1.3 wt.% and 0.1 wt.%, respectively. The positive correlation between Na and Cl suggests that part of Na occurs as NaCl. The analytical sums for this sample vary widely from 91.2 to 99.4 wt.%, probably due to the observed porosity (Fig. 5a) and the presence of water molecules in the samples [57]. The U/Si ratio along the EMPA profile is 0.99 ± 0.09 and the average chemical formula of the product with standard deviation can be written as $U_{0.99\pm0.06}Si_{0.97\pm0.07}O_4$, which is close to the expected $USiO_4$. As some uraninite was also detected from XRD analyses, the $USiO_4$ phase could be considered in equilibrium with UO_2 and Si-rich material, such as silica observed in Fig. 5d.

Sample S4 presents similar characteristic to sample S3. It contains large polyphase aggregates (Fig. 6a). The chemical composition of the darker areas range from 72.1 to 79.4 wt.% for U and from 6.7 to 7.7 wt.% for Si while the composition of the "brighter" grains

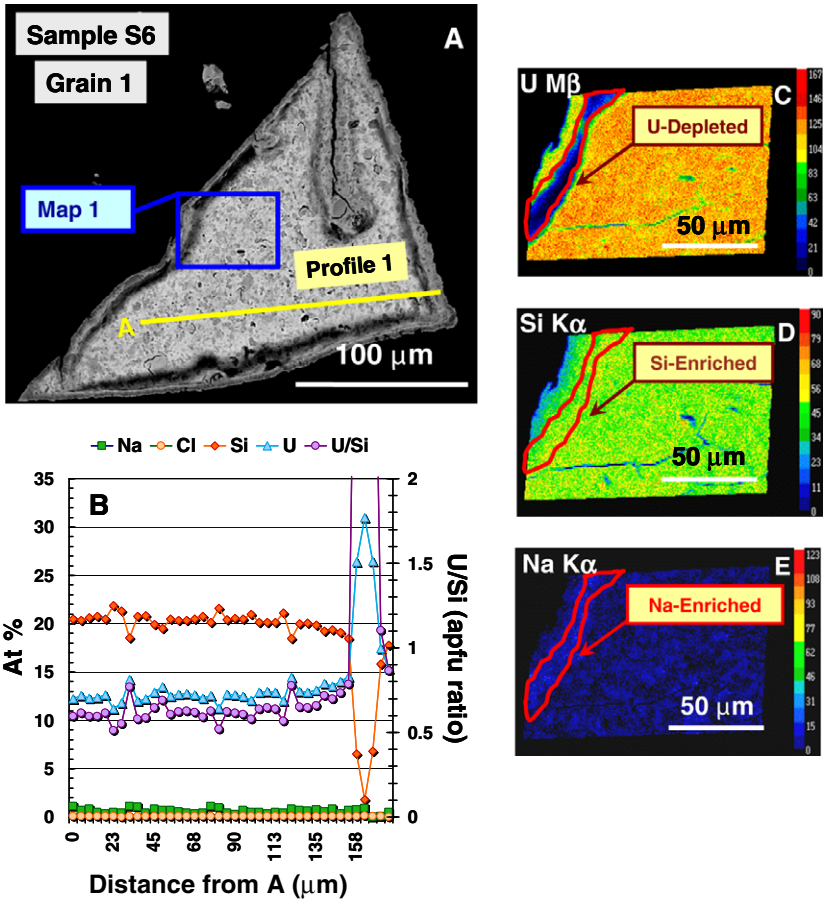

Fig. 3. (A) BSE image of coffinite grain 1 of sample S6. (B) Profile of Na, Cl, Si, and U (in atomic %) and U/Si profile (in apfu ratio) along the selected line (profile 1). The distances, in μm, are expressed from the point A. (C)–(E) Elemental maps of the selected area (Map 1): (C) U Mβ, (D) Si Kα, (E) Na Kα.

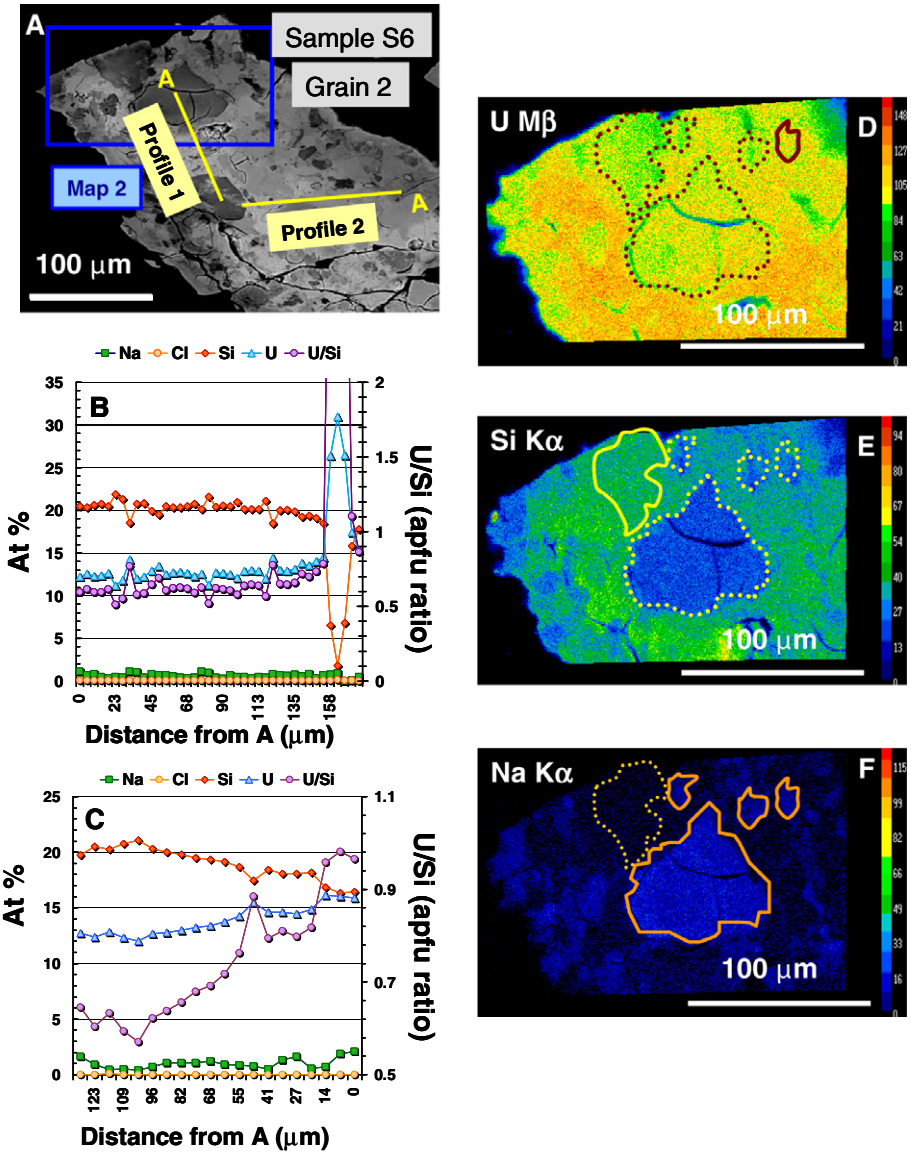

Fig. 4. (A) BSE image of coffinite grain 2 of sample S6. (B and C) Profile of Na, Cl, Si, and U (in atomic %) and U/Si profile (in apfu ratio) along the selected line; the distances, in μm, are expressed from the point A. (B) Profile 1 line. (C) Profile 2 line. (D)–(F) Elemental mapping of the selected area (Map 2): (D) U Mβ, (E) Si Kα, (F) Na Kα.

(Fig. 6b) ranges from 64.7 to 69.8 wt.% of U and from 7.8 to 9.5 wt.% of Si. The Cl concentrations are below the detection limit of 200 ppm. The U/Si ratios vary from 1.21 ± 0.07 to 0.91 ± 0.06 in "darker" and "brighter" grains, respectively, resulting in average chemical compositions of $U_{1.04\pm0.03}Si_{0.85\pm0.03}O_4$ and $U_{0.93\pm0.03}Si_{1.03\pm0.04}O_4$. The slight shift observed on the U/Si molar ratio (0.91–1.21) can be correlated with the additional presence of either a UO_2 (as shown by XRD) or a Si-rich amorphous phase (amorphous background evidenced by XRD). This is evidence that the aggregates are composed of a mixture of nanocrystalline coffinite, uraninite, and an amorphous Si-rich phase.

3.3. TEM study

Samples S6 and S4 were used for TEM analysis, as representative of samples comprising respectively 95% coffinite and a mixture of ~90 wt.% coffinite and ~10 wt.% uraninite (associated in both cases with an amorphous phase). The low-magnification TEM images reveal the presence of two kinds of nanoparticles with respect to size in samples S6 and S4: (i) ~50 nm nanoparticles of coffinite, which represent the majority of the samples (Fig. 7a and b), and (ii) 5 nm nanoparticles of uraninite (Fig. 7a and b). The SAED pattern of the larger particles confirms that the main synthesis product is coffinite (Fig. 7b). The concentric ring diffraction pattern may be due to the small size of the coffinite crystals and their random orientation, or to the presence of an amorphous phase (as suggested by XRD). Coffinite crystals of different shapes (square, rectangular, hexagonal and lozenge) are observed and represent various crystal morphologies (Fig. 7a and b). The HRTEM images show that coffinite is well crystallized and up to two directions of lattice fringes are usually observed (Fig. 8). Fourier transform analysis of the 5 nm nanoparticles reveals that they are UO_2 (Fig. 8a and b).

High-resolution images also reveal the presence of amorphous areas in both samples analyzed (Fig. 8a and b). These areas are observed on the edge of coffinite and UO_2 nanoparticles and between coffinite and uraninite. This amorphous phase may correspond to the silica-rich phase suggested by XRD and EMPA.

Table 3
Selected EMPA data from sample S6.

Na wt.%	Cl wt.%	Si wt.%	U wt.%	O wt.%*	U/Si at. ratio
Coffinite zone					
0.03	0.04	7.82	73.31	18.80	1.10
1.13	0.00	7.24	73.14	18.50	1.19
1.06	0.00	7.11	73.46	18.37	1.21
1.20	0.01	7.36	72.82	18.61	1.16
1.02	0.01	8.37	71.11	19.48	1.00
0.96	0.00	8.11	71.70	19.24	1.04
0.97	0.02	8.26	71.37	19.38	1.02
0.89	0.00	8.63	70.80	19.69	0.97
0.80	0.00	8.52	71.11	19.58	0.98
0.31	0.00	8.75	71.26	19.69	0.96
0.84 ± 0.38	0.01 ± 0.02	8.02 ± 0.60	72.01 ± 1.05	19.13 ± 0.51	1.06 ± 0.10
Si-enriched zone					
0.25	0.00	12.34	64.54	22.87	0.62
0.29	0.02	12.88	63.45	23.36	0.58
0.27	0.02	12.88	63.49	23.34	0.58
0.22	0.03	12.79	63.70	23.26	0.59
0.33	0.00	12.93	63.32	23.41	0.58
0.21	0.01	12.35	64.58	22.86	0.62
0.45	0.02	12.57	63.85	23.11	0.60
0.20	0.02	13.04	63.27	23.48	0.57
0.24	0.02	12.67	63.91	23.16	0.59
0.45	0.00	12.47	64.05	23.03	0.60
0.29 ± 0.09	0.01 ± 0.01	12.69 ± 0.25	63.82 ± 0.47	23.19 ± 0.22	0.59 ± 0.02
U-enriched zone					
1.20	0.01	7.16	73.19	18.44	1.20
1.13	0.00	7.24	73.14	18.50	1.19
1.06	0.00	7.11	73.46	18.37	1.21
1.20	0.01	7.36	72.82	18.61	1.16
1.15 ± 0.07	0.01 ± 0.01	7.22 ± 0.11	73.15 ± 0.26	18.48 ± 0.10	1.19 ± 0.02

* Oxygen amount calculated by difference.

3.4. XPS study

XPS analyses were performed on sample S6 stored in air and under N_2/H_2 gas. The deconvolutions of the main components associated with the 4*f*-core levels of uranium before and after Ar^+ ion etching are presented in Fig. 9. The main contributions are located at 380.8 ± 0.3 eV and at 391.7 ± 0.3 eV for the U-4$f_{7/2}$ and U-4$f_{5/2}$ levels, respectively. On the top surface of the sample stored in air, some traces of U(VI) were observed that were removed by Ar^+ ion etching. This confirms that the uranium content of bulk coffinite is only composed of U(IV) while U(VI) is only produced by local oxidation at the surface when sample is stored in air.

The difference of the binding energies between the main photoelectric peaks and the shake-up satellite peaks can be used as an indicator of the uranium valence state. Indeed, these peaks are usually located at higher binding energies: 6.8 eV for U(IV), 8 eV for U(V) and 4 and 10 eV for U(VI) [58]. In the case of coffinite, the observation of one satellite peak located at 6.0 eV clearly indicates that uranium is only present in the tetravalent oxidation state in the sample.

The comparison of the spectra of the 4*f*-core levels of uranium in coffinite (sample observed after Ar^+ ion etching) with those recorded for stoichiometric UO_2 or $UO_2(OH)_2$ (in which uranium is only present in the uranyl form) is presented in Fig. 10. A shift of about 1 eV toward higher binding energies is observed for U(IV) in the coffinite sample compared with the U(IV) 4*f* peak in UO_2 (U-4$f_{7/2}$ and U-4$f_{5/2}$ located at 380.0 ± 0.3 eV and 391.0 ± 0.3 eV, respectively [59]). A second contribution associated with uranium levels was observed at 382.2 ± 0.3 eV and 391.1 ± 0.3 eV in the coffinite sample stored in air. Both peaks were assigned to the U-4$f_{7/2}$ and U-4$f_{5/2}$ levels of uranium(VI), respectively, showing the oxidation of uranium(IV) to uranium(VI) at the surface of the sample;

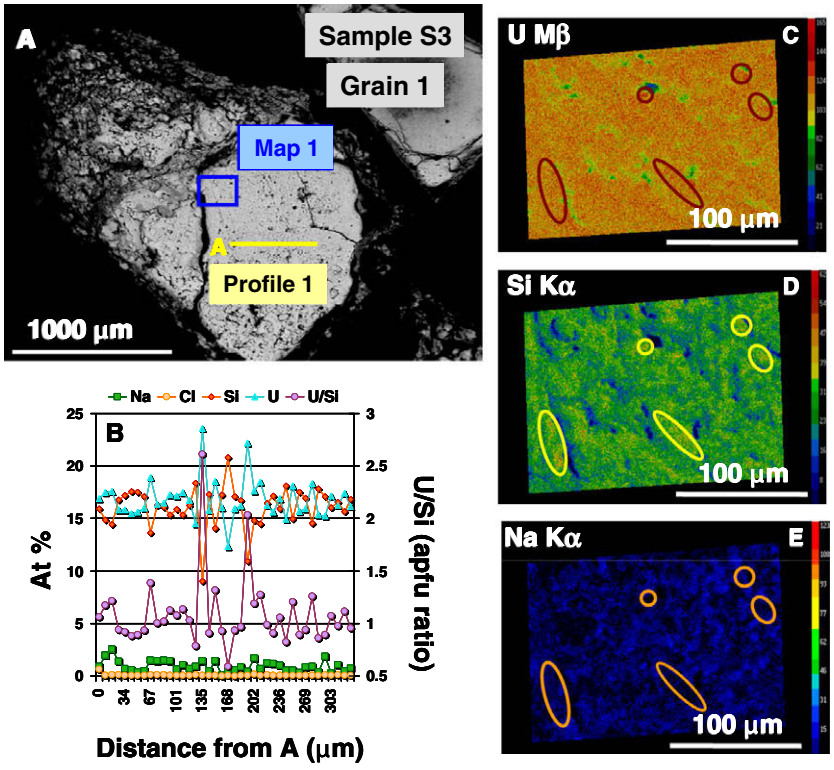

Fig. 5. (A) BSE image of coffinite grain 1 of sample S3. (B) Profile of Na, Cl, Si, and U (in atomic %) and U/Si profile (in apfu ratio) along the selected line (profile 1). The distances, in µm, are expressed from the point A. (C)–(E) Elemental mapping of the selected area (Map 1): (C) U Mβ, (D) Si Kα, (E) Na Kα.

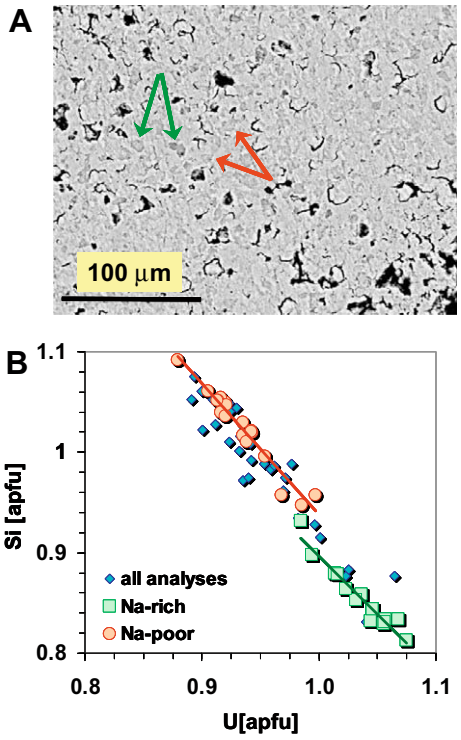

Fig. 6. (A) BSE image of the sample S4. Note polycrystalline character of the sample. "Darker" areas (green arrows) are enriched with Na and U, and depleted with Si, while "brighter" areas (red arrows) contain relatively higher concentrations of Si and lower amounts of Na and U. (B) Correlations between the U and Si elements plotted in [apfu]; green squares corresponds to the "darker" areas ($y = -1.156x + 2.052$ with $R^2 = 0.934$) and red circles to the "brighter" areas ($y = -1.131x + 2.249$ with $R^2 = 0.945$) of the BSE images (A). (For interpretation of the references to colour in this figure legend, the reader is referred to the web version of this article.)

both peaks are coupled with a satellite peak at 4 eV, which is characteristic of uranium(VI).

Ilton et al. [58] attributed the photoelectric peak U-4$f_{7/2}$ at 381.0 eV to the presence of U(V) in a mixed-valence uranium oxide compound. On the contrary, all the results obtained on our examined samples confirmed the presence of U(IV) rather than U(V), despite the shift of 1 eV observed toward higher binding energies of the U-4*f* levels. Several observations support this argument:

- First, the U(V) valence state is usually considered to be colourless and unstable, quickly disproportionating to U(IV) and U(VI). It has only been reported in mixed-valence uranium compounds (for instance, a mixture of U(IV) and U(V) or of U(VI) and U(V)). Consequently, U(V) is not expected in a phase showing an XPS spectrum composed of only one uranium valence state, as it is clearly observed for the coffinite sample obtained after Ar^+ ion etching (Fig. 9).
- Second, the U-4*f* core levels of uranium(V) are usually coupled with a shake-up satellite peak located at 8.0 eV toward higher binding energies while such a satellite peak is found at 6.0 eV in our coffinite samples, which is close to the value observed for uranium(IV). The satellite peaks observed for $USiO_4$ and UO_2 are shown in Fig. 10.
- Third, the ratio between the intensities of the U-5*f* and U-4*f* levels can be used to check for the presence of uranium(IV) or uranium(V) since it is directly related to the ratio between the two uranium oxidation states: the number of 5*f* electrons (valence electrons) decreases when increasing the oxidation state of uranium while the number of 4*f* electrons (core electrons) remains constant. In this context, the ratio of U-5*f*/U-4*f* intensities was found to be 0.012 for stoichiometric UO_2 (for our analysis conditions, i.e. pass energy, X-ray source). Using the same experimental conditions, the peak ratio determined for coffinite obtained after Ar^+ ion etching was also equal to 0.012, confirming the presence of only uranium(IV).

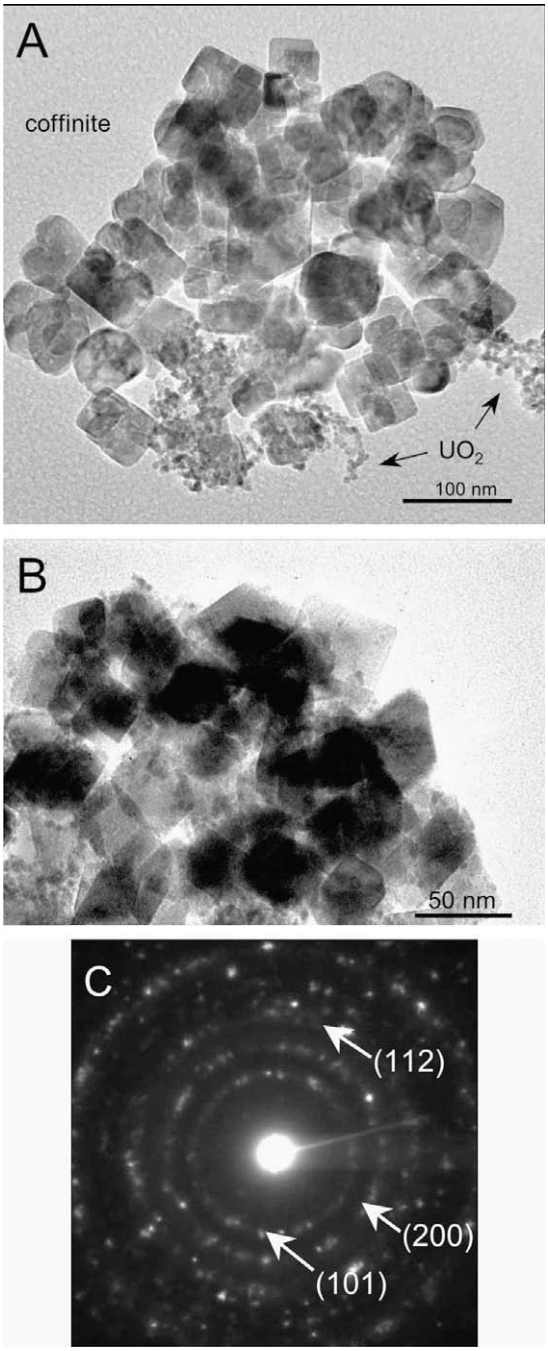

Fig. 7. TEM observation of coffinite and uraninite aggregates in samples S6 (A) and sample S4 (B) associated with SAED pattern of coffinite.

As previously mentioned, a direct comparison of the XPS spectra of UO_2 and $USiO_4$ revealed a shift of about 1 eV in the uranium binding energies between the two compounds. Comparable shifts have already been observed when comparing ZrO_2 and $ZrSiO_4$; Guittet et al. [60] observed the same shift (1.0 eV) for the 3*d* levels of zirconium in ZrO_2 and $ZrSiO_4$ (3$d_{5/2}$ level observed at 181.9 and 182.95 eV, respectively). According to the literature, Guittet et al.

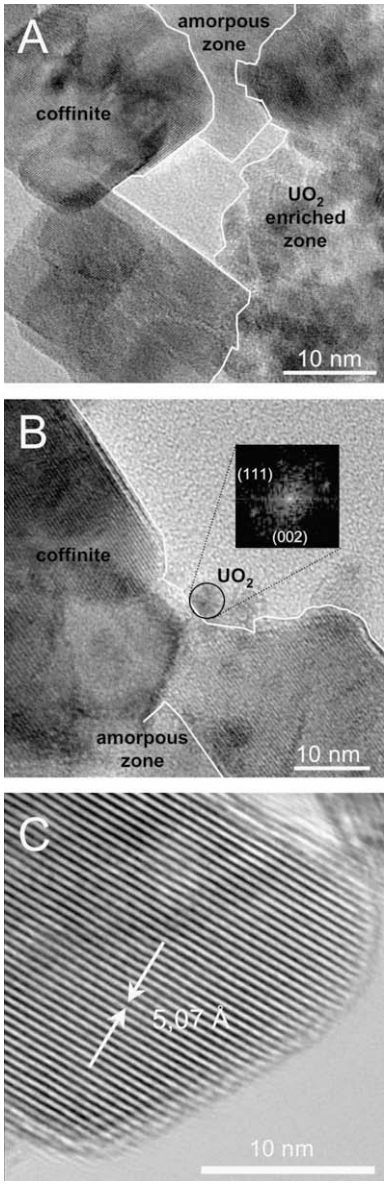

Fig. 8. HRTEM images of the assemblage of coffinite, uraninite and amorphous phase of sample S6 (A) and sample S4 (B) (note the presence of 50 and 5 nm nanoparticles; Fourier transforms of the HRTEM images of larger and smaller nanoparticles identified to coffinite and uraninite, respectively; note also the large amorphous domain) and isolated coffinite particle following the [1 1 1] axis (C).

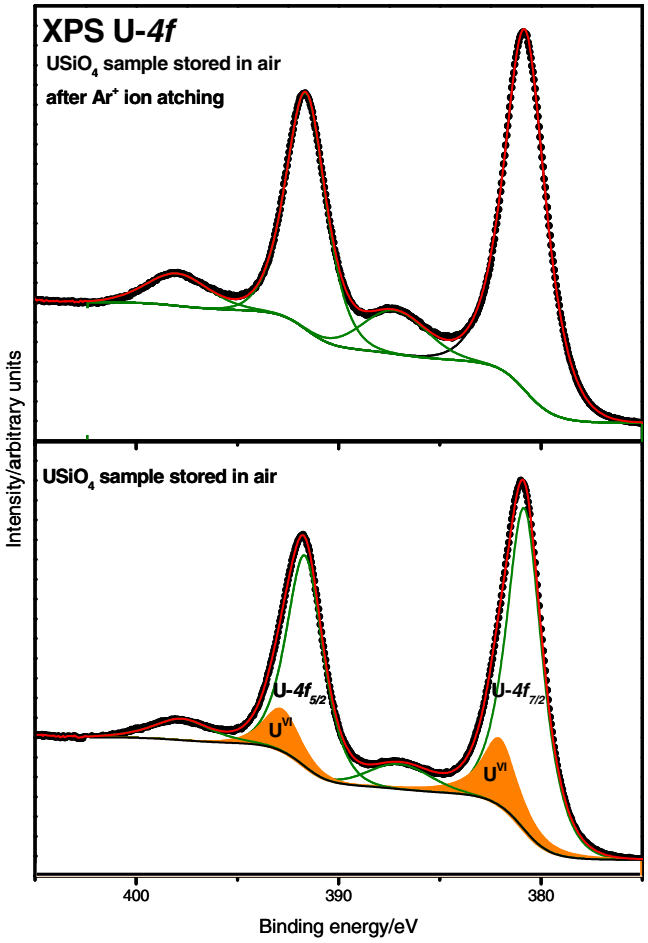

Fig. 9. Deconvolution of the 4*f*-core levels of uranium in coffinite stored in air and stored in air after ion etching (Ar^+ ions with an incident energy of 3 keV, target current of 1 μA).

has showed that the calculated charge on Zr is larger in $ZrSiO_4$ than in ZrO_2 (Zr being more ionic than Si in $ZrSiO_4$). On the basis of the similarities between $ZrSiO_4$ and $USiO_4$, such an explanation could be proposed to explain the binding energy shift observed for the U-4*f* levels between $USiO_4$ and UO_2. However, some calculations based, for example, on density functional theory, should be performed to support this assumption.

The 2*p*-core levels of silicon in coffinite samples lead to some interference with the 5*d*-core levels of uranium. Consequently, the 2*s*-core level of silicon was studied to confirm the presence of silicate in the prepared coffinite samples in order to exclude the presence of a mixture of UO_2 and SiO_2. While the Si-2*s* peak of silicon induces no interference, only few data describing the binding energies versus the chemical silicon environment are available in literature. A comparison of the 2*s*-core level of silicon in SiO_2, $ZrSiO_4$ and $USiO_4$ is given in Fig. 11. While the binding energy associated with this level is found to be 154.7 ± 0.3 eV in SiO_2, it reaches 153.0 ± 0.3 eV in $ZrSiO_4$ and 153.6 ± 0.3 eV in coffinite. Even though the difference in the binding energy is lower for $USiO_4$, probably due to the difference in electronegativity of zirconium and uranium that can affect the Si–O edges, the presence of silicate entities is clearly demonstrated. This result appears as a good confirmation of the U-4*f* analyses excluding the presence of UO_2.

4. Discussion

This paper describes a reproducible protocol for coffinite synthesis. All syntheses performed at starting pH value between 8 and 9 led to the formation of coffinite as the major phase. HRTEM, EMPA and XRD analyses confirm that the samples prepared using the above conditions are composed of: (i) tetragonal crystals of coffinite (~50 nm in size) as the major constituent; (ii) 2–5 nm particles of cubic UO_2 and (iii) an amorphous Si-rich phase as minor constituents (Fig. 8a and b). The amount of UO_2 and Si-rich amorphous phase was found to vary from sample to sample as evidenced by XRD and TEM. The initial pH value is a determining parameter controlling the formation of coffinite. At pH 12, the redox conditions inhibit the formation of coffinite and favor precipitation of UO_3 and Na_2SiO_3, as shown for sample S1.

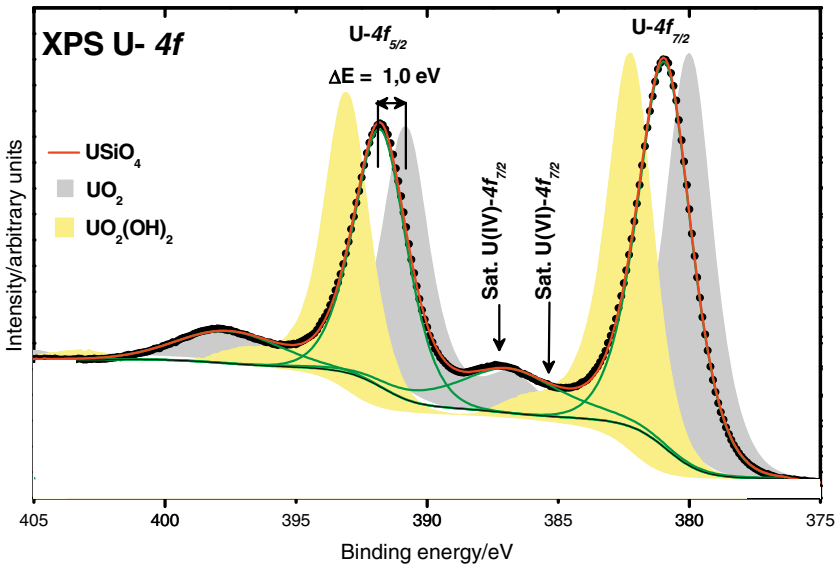

Fig. 10. Comparison of the 4*f*-core levels of uranium for the sample of coffinite (S6) after Ar^+ ion etching, with stoichiometric UO_2 and $UO_2(OH)_2$.

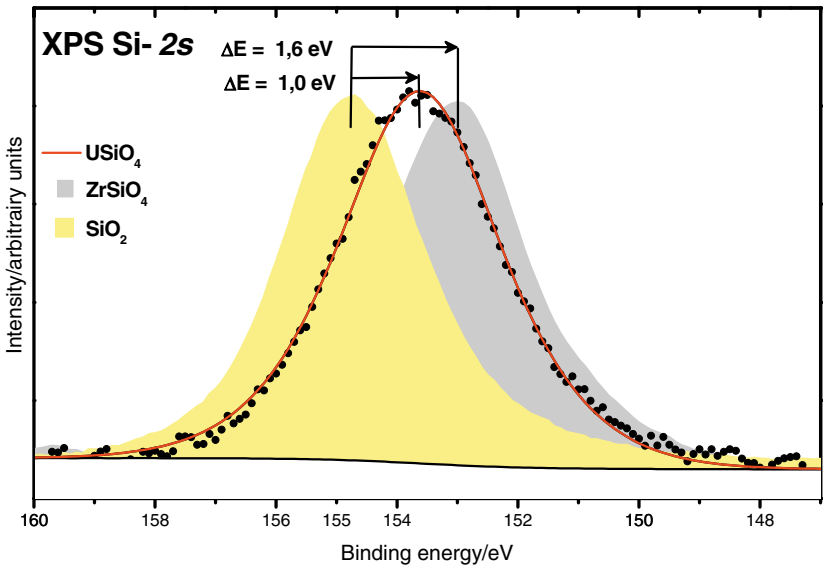

Fig. 11. Comparison of the 2*s*-core level of silicon for the sample of coffinite (S6) after Ar^+ ion etching, with $ZrSiO_4$ and SiO_2.

No coffinite was detected by XRD in sample S5 coupling a low heating rate during synthesis (60 °C/h) with mechanical stirring and a pressure rise to 10 bars during heating. The increased pressure probably precludes the formation of coffinite in favor of UO_2 and Si-rich amorphous phases (sample S5, Fig. 2). This could explain the unsuccessful syntheses of coffinite under higher pressure [46,51]. Contamination of the initial UCl_4 solution with 5% U(VI) could also lead to UO_2 formation [46].

The direct comparison between samples S3 and S6 evidences that a longer heating time (84 h vs. 24 h, respectively) favors the formation of a higher proportion of UO_2, which seems to indicate that coffinite decomposes over time to UO_2 and Si-rich amorphous phase at 250 °C.

5. Conclusion

A reproducible protocol for synthesizing coffinite samples has been described. The successful synthesis of coffinite depends on several parameters: (i) coffinite precipitates only if uranium solution is added to the silica solution (and not in the reverse order); (ii) acidic conditions (pH < 8) favor UO_2 formation, while UO_3 forms at higher pH values (e.g. pH 12); (iii) the formation of coffinite is also limited by temperature and pressure (T > 360 °C and/or P > 40 bars result in UO_2 precipitation). HRTEM studies reveal that synthetic coffinite is always associated with small quantities of nanocrystalline uraninite and an amorphous phase in spite of the fact that XRD analyses only show coffinite (sample S6). However, the parameters controlling the quantity of UO_2 and amorphous gel were not determined. The small size of coffinite and UO_2 nanoparticles, ~50 and 4 nm, respectively, precludes efficient separation of these materials using conventional methods such as gravimetry in liquid media, centrifugation or filtration, sieving, etc. Furthermore, reference positions for core levels of U-4$f_{7/2}$, U-4$f_{5/2}$ and Si-2*s* in coffinite have been determined by XPS to be 380.8 ± 0.3 eV, 397.7 ± 0.3 eV, and 153.6 ± 0.3 eV, respectively.

Acknowledgements

This work was supported by the Office of Basic Energy Sciences of the US Department of Energy, through Grant No. DE-FG02-06ER15783 and the NSF NIRT program (EAR-0403732). Support for Veronique Robit-Pointeau was provided in part by the Commissariat à L'Énergie Atomique (CEA – France).

References

[1] L.H. Johnson, N.C. Garisto, S. Stroes-Gascoyne, Proc. Waste Manage. (1985) 479.
[2] C. Ferry, C. Poinssot, C. Cappelaere, L. Desgranges, C. Jégou, F. Miserque, J.P. Piron, D. Roudil, J.M. Gras, J. Nucl. Mater. 352 (2006) 246.
[3] C. Jégou, B. Muzeau, V. Broudic, S. Peuget, A. Poulesquen, D. Roudil, C. Corbel, J. Nucl. Mater. 341 (2005) 62.
[4] G. Sattonnay, C. Ardois, C. Corbel, J.F. Lucchini, M.F. Barthe, F. Garrido, D. Gosset, J. Nucl. Mater. 288 (2001) 11.
[5] C. Poinssot, C. Ferry, A. Poulesquen, Mater. Res. Soc. Symp. Proc. 985 (2006).
[6] C. Poinssot, J.M. Gras, Mater. Res. Soc. Symp. Proc. 1124, in press.
[7] M. Amme, T. Wiss, H. Thiele, P. Boulet, H. Lang, J. Nucl. Mater. 341 (2005) 209.
[8] P. Wersin, M.F. Hochella Jr., P. Persson, G. Redden, J.O. Leckie, D.W. Harris, Geochim. Cosmochim. Acta 58 (1994) 2829.
[9] R. Guillaumont, T. Fanghänel, J. Fuger, I. Grenthe, V. Neck, D.A. Palmer, M.H. Rand, Update on the Chemical Thermodynamics of Uranium, Neptunium, Plutonium, Americium and Technetium, NEA-OCDE, 2003, p. 5.
[10] M.B. Goldhaber, B.S. Hemingway, A. Mohagheghi, R.L. Reynolds, H.R. Northrop, Bull. Mineral. 110 (1987) 131.
[11] G. Smits, Can. Mineral. 27 (1989) 643.
[12] J. Janeczek, R.C. Ewing, Mater. Res. Soc. Symp. Proc. 257 (1992) 497.
[13] J. Janeczek, R.C. Ewing, J. Nucl. Mater. 190 (1992) 157.
[14] V. Savary, M. Pagel, Geochim. Cosmochim. Acta 61 (1997) 4479.
[15] R. Bros, H. Hidaka, T. Ohnuki, Appl. Geochem. 18 (2003) 1807.
[16] J. Janeczek, R.C. Ewing, V.M. Oversby, L.O. Werme, J. Nucl. Mater. 238 (1996) 121.
[17] J. Janeczek, R.C. Ewing, Geochim. Cosmochim. Acta 59 (1995) 1917.
[18] L. Pourcelot, F. Gauthier-Lafaye, Chem. Geol. 157 (1999) 155.
[19] K.A. Jensen, J. Janeczek, R.C. Ewing, P. Stille, F. Gauthier-Lafaye, S. Salah, Mater. Res. Soc. Symp. Proc. 608 (2000) 525.
[20] J. Cramer, J. Smellie, Final Report of the AEL/SKB Cigar Lake Analog Study, SKB Report TR 94-04, 1984.
[21] M. Fayek, J. Janeczek, R.C. Ewing, Appl. Geochem. 12 (1997) 549.
[22] R.J. Finch, T. Murakami, in: P.C. Burns, R.J. Finch (Eds.), Uranium: Mineralogy, Geochemistry and the Environment, Rev. Min. 38 (1999) 91.
[23] M. Fayek, T.M. Harisson, R.C. Ewing, M. Grove, C.D. Coath, Chem. Geol. 185 (2002) 205.
[24] Z.B. Chen, F.M. Zhao, W.D. Xiang, Y.H. Chen, Acta Geol. Sin. 74 (2000) 587.
[25] V.M. Goldschmidt, Geochemistry, Clarendon Press, Oxford, 1954.
[26] L.R. Stieff, Sciences 121 (1955) 608.
[27] L.R. Stieff, Am. Mineral. 41 (1956) 675.
[28] L.H. Fuchs, E. Gebert, Am. Mineral. 43 (1958) 243.
[29] V.T. Dubinchuk, I.S. Naumova, I.Y. Kravtsova, G.A. Sidorenko, Mineral. Zh. 3 (1981) 81.
[30] J.A. Speer, Rev. Mineral. 5 (1980) 113.
[31] M. Taylor, E. Gebert, Am. Mineral. 43 (1958) 243.
[32] J. Janeczek, R.C. Ewing, J. Nucl. Mater. 190 (1992) 128.
[33] L.H. Fuchs, H.R. Hoekstra, Am. Mineral. 44 (1959) 1057.
[34] A.M. Abdel-Gawrad, P.F. Kerr, Am. Mineral. 46 (1961) 402.
[35] L.N. Belova, G.A. Tananaeva, K.E. Frolova, Atom. Energy 27 (1969) 61.
[36] P. Zimmer, Mémoire Cregu n°12, Géologie et Géochimie de l'uranium, Nancy, 1986.
[37] D.G. Brookins, Abstr. Bull. Am. Assoc. Petr. Geol. 95 (1975) 905 (New Mexico).
[38] B.S. Hemingway, Open File Report, 1982, p. 82.
[39] J.L. Fleche, Phys. Rev. B 65 (2002) 1.
[40] D. Langmuir, Geochim. Cosmochim. Acta 42 (1978) 547.
[41] V. Robit-Pointeau, C. Poinssot, P. Vitorge, B. Grambow, D. Cui, K. Spahiu, H. Catalette, Mater. Res. Soc. Symp. Proc. 932 (2006) 489.
[42] B. Grambow, E. Giffaut, Mater. Res. Soc. Symp. Proc. 932 (2006) 55.
[43] C. Keller, Über dir Fstkörperchemie der Actiniden-Oxide, KFK 225, Karlsruhe, 1964.
[44] J. Mulak, J. Solid State Chem. 21 (1977) 117.
[45] F.A. Mumpton, R. Roy, Geochim. Cosmochim. Acta 21 (1961) 217.
[46] V. Robit-Pointeau, Etude des phases néoformées lors de la dissolution du combustible nucléaire en condition de stockage géologique profond: influence des ions silicates. PhD thesis, University of Paris-Sud-11, 2005.
[47] J.A. Tossel, Geochim. Cosmochim. Acta 69 (2005) 283.
[48] A.P. Deditius, S. Utsunomiya, R.C. Ewing, Chem. Geol. 251 (2008) 33.
[49] F. Pishva, Synthesis of Uranium Silicate, East Texas State University, Master Degree Report, 1991.
[50] M. Amme, B. Renker, B. Schmid, M.P. Feth, H. Bertagnolli, W. Döbelin, J. Nucl. Mater. 306 (2002) 202.
[51] P. Zimmer, CREGU Report, Nancy, France, 1981, p. 81.
[52] C. Nguyen, Géochimie de l'uranium: Gisements, Analogues naturels, Environnement, Nancy, 2003, p. 259.
[53] N. Clavier, N. Dacheux, P. Martinez, V. Brandel, R. Podor, P. Le Coustumer, J. Nucl. Mater. 335 (2004) 397.
[54] N. Dacheux, V. Brandel, M. Genet, New J. Chem. 19 (1995) 15.
[55] N. Dacheux, V. Brandel, M. Genet, New J. Chem. 19 (1995) 1029.
[56] T.J.B. Holland, S.A.T. Redfern, Mineral. Mag. 61 (1997) 65.
[57] F.X. Zhang, V. Pointeau, L.C. Shuller, D.M. Reaman, M. Lang, Zhenxian Liu, Jingzhu Hu, W.R. Panero, U. Becker, C. Poinssot, R.C. Ewing, Am. Mineral. 94 (2009) 916.
[58] E.S. Ilton, J.F. François, P.S. Bagus, Surf. Sci. 601 (2007) 908.
[59] F. Miserque, Photoelectron Spectroscopy and Electrochemical Studies of Uranium Oxides and Nitrides Thin Films, PhD, Namur, 2001, ISBN:2-87037-345-7.
[60] M.J. Guittet, J.P. Crocombette, M. Gautier-Soyer, Phys. Rev. B (2001) 63.